Open Access Indonesian Journal of Medical Reviews
Volume 6, Issue 5, 2026 | Article ID: 933 | Pages: 392–403 | e-ISSN 2807-6257
OAIJMR

ORIGINAL RESEARCH

Unequal Per-Grade Loss of Macular Ganglion Cell–Inner Plexiform Layer Thickness in Non-Proliferative Diabetic Retinopathy: An Indonesian Cross-Sectional Study

Sarah Yasmin Ramadhanti[1*], Weni Helvinda[2], Khalilul Rahman[2]

[1]Ophthalmology Resident, Universitas Andalas/M. Djamil General Hospital, Padang, Indonesia
[2]Staff, Vitreoretina Subdivision, M. Djamil General Hospital, Padang, Indonesia

ARTICLE INFO

Article history
Received: July 19, 2026
Revised: August 15, 2026
Accepted: September 2, 2026
Available Online: September 7, 2026
Published: September 8, 2026

Keywords
Diabetic retinopathy; Indonesia; optical coherence tomography; retinal degeneration; retinal ganglion cells

***Corresponding author**
Sarah Yasmin Ramadhanti
E-mail: syrsarah@gmail.com

DOI
https://doi.org/10.37275/oaijmr.v6i5.933

ABSTRACT

Background: Diabetic retinopathy is a neurovascular disease in which neurodegeneration accompanies microvascular injury. How ganglion cell–inner plexiform layer (GCL–IPL) loss is distributed across non-proliferative diabetic retinopathy (NPDR) severity is unsettled; Indonesian data are scarce.

Objective: To quantify mean macular GCL–IPL thickness across mild, moderate and severe NPDR; test whether successive per-grade decrements are equal and scale-dependent; characterise discrimination between grades; and bound the influence of aggregate-data uncertainty and confounding.

Methods: Cross-sectional analysis of 32 eyes of 29 consecutive adults with mild, moderate or severe NPDR without macular oedema at Dr. M. Djamil General Hospital, Padang (2023–2025). Mean macular GCL–IPL thickness was measured by spectral-domain optical coherence tomography. Only aggregate data existed, so sharp bounds came from exhaustively enumerating every eye-level dataset compatible with the published summaries and the reported normality test.

Result: GCL–IPL thickness fell from 86.0 ± 3.63 µm (mild) to 71.0 ± 4.71 µm (moderate) and 63.8 ± 3.39 µm (severe); $F(2, 29) = 86.288$, $p < 0.001$, $\eta^2 = 0.856$ (95% CI 0.724–0.900). All pairwise contrasts were significant (Bonferroni $p \leq 0.0008$). The per-grade steps were unequal: mild→moderate lost 15.0 µm against 7.2 µm for moderate→severe, a difference of 7.8 µm (95% CI 1.75–13.85, $p = 0.013$). That asymmetry is a property of the equal-interval grade score and disappears under ETDRS-level scoring ($p = 0.759$). Mild and severe eyes separated completely in every admissible dataset (area under the curve 1.000); moderate versus severe, 0.827–0.964.

Conclusion: GCL–IPL thickness tracks NPDR severity steeply, but the apparent front-loading of loss is scale-dependent and must not be read as biology. The mild-grade mean lay within the published normative band — an interval built for individual eyes, not for group means — so these data show a gradient, not pre-clinical thinning.

1. Introduction

Diabetic retinopathy remains the leading cause of preventable blindness in working-age adults and the only major cause of vision loss whose age-standardised prevalence continues to rise.[1,2] The International Diabetes Federation places global diabetes prevalence at 589 million in 2024, projected to reach 853 million by 2050,[2] while a pooled analysis of population-based studies estimated 103.12 million people with diabetic retinopathy in 2020, rising to 160.50 million by 2045 and affecting 22.27% of all people with diabetes.[1] Indonesia carries a substantial share of that burden: the national Riskesdas survey put diabetes prevalence at 10.9% among adults aged 15 years and older,[3] and retinopathy complicates a considerable minority of those cases.[4,5] Diagnostic capacity is concentrated in a small number of provincial referral hospitals,[3,4] and the strategic response advocated for Asia combines risk-stratified review intervals with task-shifted and, increasingly, automated grading.[5-7]

The conceptual model of the disease has changed. Diabetic retinopathy is no longer regarded as a purely microvascular disorder but as a disease of the retinal neurovascular unit, in which neuronal, glial and vascular compartments fail together.[8-10] Chronic hyperglycaemia drives polyol flux, accumulation of advanced glycation end-products with receptor-mediated signalling, protein kinase C activation and mitochondrial reactive oxygen species; the same cascades that injure pericytes and the endothelial barrier also trigger ganglion-cell apoptosis.[11-13] Loss of glutamate clearance by Müller cells adds an excitotoxic component, and microglial activation amplifies both limbs.[8,9] It has been argued that any modern staging system must therefore capture neural as well as vascular change.[14,15]

The macular ganglion cell–inner plexiform layer (GCL–IPL) is the natural structural readout of that neuronal compartment. Roughly half of all retinal ganglion cells lie within the macula, and spectral-domain optical coherence tomography (SD-OCT) with automated segmentation quantifies the combined ganglion-cell somata and their synaptic layer reproducibly and non-invasively.[16,17] Landmark work has shown progressive GCL–IPL and nerve-fibre-layer loss in people with diabetes before any retinopathy is visible,[18,19] functional and structural biomarkers of neurodegeneration already measurable in pre-clinical and early retinopathy,[20] and parallel progression of neuroretinal thinning and capillary dropout on OCT angiography.[14] More recent series have extended the observation to newly diagnosed diabetes, to prolonged diabetes without retinopathy, and to eyes with established NPDR without macular oedema.[21-25] Series that stratify by retinopathy grade rather than by its presence alone likewise report graded thinning, as do analyses that segment all inner-retinal layers simultaneously.[26-29] Analyses that model neurodegeneration on sociodemographic, metabolic and morphological predictors reach the same conclusion for the pre-clinical stage.[30]

A smaller but rapidly growing body of work has gone further and stratified the neuronal measurement by retinopathy grade rather than by its mere presence. Sung and colleagues showed that the ratio of GCL–IPL thickness to superficial vessel density tracks progression;[31] Kaushal and colleagues profiled macular GCL–IPL in diabetic eyes with and without retinopathy;[32] Pemp and colleagues linked neurovascular dysfunction to inner retinal

layer thickness specifically within non-proliferative disease;[33] and Wu reported reduced retinal layer thickness across mild to moderate NPDR.[34] Lee and colleagues graded nerve-fibre-layer damage by retinopathy severity,[35] and Wang and colleagues have proposed temporal-sector nerve-fibre-layer thickening — a change opposite in direction to macular ganglion-cell loss — as a structural marker of severity.[36] Indonesian series point the same way: Ulhaq and colleagues found nerve-fibre-layer thickness useful for grading severity,[37] and two North Sumatran cohorts related retinopathy grade to nerve-fibre-layer thickness and to diabetes duration.[38,39] Bansal and colleagues report both peripapillary and macular measurements in the same eyes.[40]

What that literature has not settled is how the loss is distributed across severity. Almost every study either contrasts diabetes with health, or contrasts eyes with and without retinopathy, and then reports a correlation coefficient. A correlation answers whether thickness falls as severity rises; it cannot say whether each clinical step costs the same. That distinction matters, because clinicians act on grades rather than on a continuous severity scale: if one transition costs far more neuroretinal tissue than the next, that is the transition at which surveillance and metabolic intervention are most valuable. The same question arises wherever the retinal neural compartment is proposed as a pharmacological target, because any such treatment presupposes that neurodegeneration is still available to be prevented rather than already accomplished.[18] Within-grade heterogeneity is well documented for the vascular limb: mild NPDR contains phenotypes with very different progression risks,[6,41] and systematic reviews of imaging in diabetes without retinopathy reach the same conclusion for the pre-clinical stage.[42,43]

This study was conducted at the Vitreoretinal Subdivision of Dr. M. Djamil General Hospital, Padang, the tertiary referral centre for West Sumatra. Its aims were, first, to quantify mean macular GCL–IPL thickness across ETDRS-graded mild, moderate and severe NPDR in an Indonesian cohort; second, to test whether the per-grade decrements are equal, and to establish how far any answer depends on the numerical scale assigned to the grades; third, to characterise how well GCL–IPL discriminates between grades; and fourth, to establish how much of the observed gradient could survive worst-case confounding by age, diabetes duration and glycaemic control. Because the analysis was necessarily built on aggregate summaries rather than a released record-level file, every rank-based quantity is reported as a sharp identified interval derived by exhaustive enumeration rather than as a single point estimate whose provenance cannot be checked.

2. Methods

Design and setting

This was a retrospective, single-centre, cross-sectional study reported in accordance with the STROBE statement for observational research.[44] Data were drawn from the electronic medical records of the Vitreoretinal Subdivision, Ophthalmology Clinic, Dr. M. Djamil General Hospital, Padang, Indonesia, covering consecutive attendances between January 2023 and December 2025. Dr. M. Djamil General Hospital is the West Sumatran provincial referral hospital and the teaching hospital of the Faculty of Medicine, Andalas University.

Participants and eligibility

Total (consecutive) sampling was applied to the whole eligible record set for the study window; no sampling fraction was imposed. Eyes were eligible when (i) a vitreoretinal consultant had recorded a diagnosis of mild, moderate or severe NPDR, (ii) the record was complete for age, sex, diabetes duration, visual acuity and glycated haemoglobin (HbA1c), and (iii) a macular ganglion-cell analysis scan from the first visit was available. Eyes were excluded for any coexisting condition capable of altering inner-retinal thickness independently of diabetes — glaucoma, hypertensive retinopathy, retinal vein occlusion or age-related macular degeneration — for concomitant diabetic macular oedema, and for an OCT signal strength below 6. The oedema exclusion matters: intraretinal fluid inflates segmented inner-retinal thickness and would bias a severity gradient in the opposite direction to the hypothesis. The number of records screened before exclusions was not recorded in the source documentation and is not reconstructed here; participant flow is summarised in Figure 1 with that gap shown explicitly.

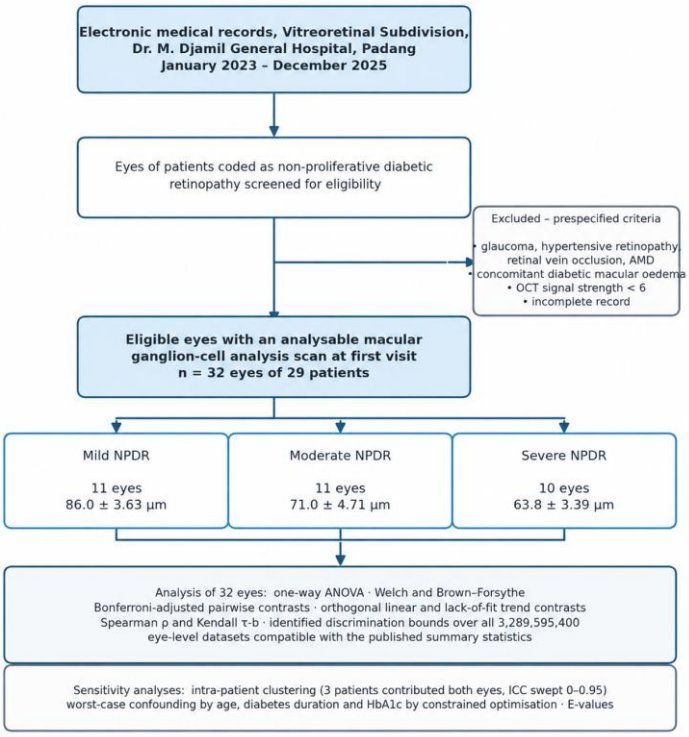

Figure 1. *Participant flow and analysis plan. Consecutive records from the Vitreoretinal Subdivision, Dr. M. Djamil General Hospital, Padang, January 2023 to December 2025, yielded 32 eligible eyes of 29 patients across three ETDRS severity grades. The number screened before exclusions was not documented in the source record set and is shown as unknown rather than reconstructed. The lower panels list the primary and sensitivity analyses applied.*

Grading and measurement

NPDR severity was graded on dilated fundoscopy by a vitreoretinal consultant using ETDRS criteria: mild denotes microaneurysms only; moderate denotes additional intraretinal haemorrhages, hard exudates or cotton-wool spots; severe is defined by the 4-2-1 rule, namely extensive intraretinal haemorrhages in four quadrants, venous beading in two quadrants, or intraretinal microvascular abnormalities in one quadrant, in the absence of neovascularisation.[45,46] Grading was performed by a single consultant; no second reader was available, so no agreement statistic can be reported. The outcome variable was mean macular GCL–IPL thickness in micrometres, taken from the ganglion cell analysis protocol of the SD-OCT device, which reports the average over the elliptical annulus centred on the fovea on a 1 µm integer grid. Neither the device model nor the segmentation software version was documented in the record set, which limits transfer of any absolute threshold to other platforms.[16,47] Covariates recorded were age, sex, diabetes duration and HbA1c; retinal microvascular indices from angiography, which several groups have shown to grade in parallel with layer thickness,[48-50] were not available.

Sample size and precision

The study was a complete enumeration of eligible records rather than a sample sized in advance, so a conventional a-priori calculation does not apply; the achievable precision is reported instead. With 32 eyes distributed 11/11/10 across three grades, a one-way analysis of variance at $\alpha = 0.05$ has 80% power to detect Cohen's $f = 0.578$, equivalent to $\eta^2 = 0.251$. The study was therefore powered only for large effects, and any null result would have been uninformative. For the closest pair of grades, the Bonferroni-adjusted minimum detectable difference was 5.89 µm. Estimating the moderate–severe difference to a half-width of ± 2 µm would require 33 eyes per grade. These figures are reported so that readers can judge which findings below are well determined and which are not.

Statistical analysis

Analyses were carried out in Python 3.11 with NumPy 2.4 and SciPy 1.17; the complete analysis script accompanies this article. Group means were compared by one-way analysis of variance, with Welch's and Brown–Forsythe's variance-robust tests reported alongside because group standard deviations differed. Pairwise contrasts used the pooled within-group mean square with Bonferroni adjustment across the three comparisons, and Bonferroni-adjusted confidence intervals accompany every mean difference. Effect sizes were η^2 with a non-central F confidence interval for the omnibus test and Hedges' g for each pair. Discrimination between grades was expressed as the probabilistic index (the area under the receiver-operating characteristic curve) and tested against 0.5 by exact permutation over all 352,716 splits rather than by the DeLong variance, which is anti-conservative at these sample sizes.

The distribution of loss across grades was examined by partitioning the between-group sum of squares. A weighted least-squares regression of grade mean on a numerical severity score, with group sizes as weights, yields a linear component; the residual is a lack-of-fit component on one degree of freedom. The contrast that carries it, $c = (1, -2, 1)$, is the unique contrast orthogonal to both the constant and an equally spaced score vector, and equals the difference between the two successive decrements. Because that orthogonality is a property of the score vector and not of the disease, the whole analysis was repeated under three alternative scorings — the ETDRS severity levels 20/43/53, an alternative 20/43/47, and a logarithmic scale — and the score value that would make the fit exactly linear was solved for. This scale-sensitivity analysis is reported in full because it changes the interpretation.[45,46] The linear component was tested with the correctly weighted contrast proportional to $n_g(x_g - \bar{x}_w)$, which alone reproduces the regression sum of squares and is exactly orthogonal to the lack-of-fit contrast at unequal group sizes; the naive (−1, 0, 1) contrast is neither.

Recovery of the eye-level data and identified bounds

Record-level measurements were not available for re-analysis; only the published group means, standard deviations and counts were. Rather than treat those summaries as if they determined a unique dataset, the full set of datasets consistent with them was constructed explicitly. Because the device reports thickness on a 1 µm integer grid, each grade corresponds to a set of integers with a fixed sum and a fixed sum of squared deviations. The GRIM granularity test was applied to each mean[51] and the GRIMMER test to each standard deviation. GRIM has essentially no power at these sample sizes — with n = 11 and a mean printed to one decimal place the granularity of attainable means is 1/11, narrower than the reporting interval, so the test cannot fail — and it is reported only for completeness. GRIMMER is the informative test here, and it pins the sum of squared deviations uniquely in each grade: 132 for mild, 222 for moderate and 103.6 for severe. Their total, 457.6, is therefore the exact within-group sum of squares, from which the analysis of variance can be reconstructed without any rounding allowance.

Exhaustive recursive enumeration under those constraints produced 1,300 admissible multisets for mild NPDR, 5,738 for moderate and 441 for severe. The source additionally reports that Shapiro–Wilk testing was non-significant in every grade; imposing that condition removes the multisets incompatible with it and leaves 960, 4,595 and 330 respectively, or 1,455,696,000 complete eye-level datasets against 3,289,595,400 without it. Every enumerated solution was re-checked against all constraints before use. Any statistic that depends only on the group means and variances is identical across the family and is reported as a point estimate. Any statistic that depends on the ordering within grades — Spearman's ρ, Kendall's τ-b, the Mann–Whitney statistic, the area under the curve, and any threshold's sensitivity and specificity — is not identified by the published summaries and is reported as the sharp interval attained over the family, with the normality-constrained interval as the primary result and the unconstrained interval as a conservative alternative. For the pairwise Mann–Whitney statistic the objective is bilinear in the two grades' count vectors, so its extremes were obtained exactly rather than by sampling, and both extremal pairs were re-verified by direct pairwise counting.

Sensitivity analyses

Three patients contributed both eyes, so the 32 eyes are not fully independent. Cluster sizes are unequal (26 singletons and 3 pairs), so the design effect was computed with Kish's effective cluster size, the ratio of the sum of squared cluster sizes to the sum of cluster sizes, which is 1.1875 rather than the naive mean of 1.1034; the omnibus F was deflated by the design effect and not only its degrees of freedom. Worst-case confounding was bounded by constrained optimisation: for each covariate, the largest value of each contrast compatible with that covariate's reported total standard deviation was found by sequential least-squares programming, cross-checked against the closed form, and the active constraint verified at the optimum; the resulting spread was multiplied by an external estimate of that covariate's association with GCL–IPL thickness.[16,25] The bound was computed for the mild–severe contrast, the moderate–severe contrast and, critically, for the lack-of-fit contrast itself. E-values were computed for every pairwise contrast at the point estimate, at the 95% limit and at the Bonferroni-consistent limit.[52] Group means were finally benchmarked against the normative GCL–IPL range quoted in the source report.

Ethical approval

This study received ethical approval from CMHC Research Center, Indonesia (Ref No CMHC/VI/2023/099).

3. Results

Participants

Thirty-two eyes of 29 patients met all criteria: 11 eyes with mild NPDR, 11 with moderate NPDR and 10 with severe NPDR;

the flow of records from the clinic database to the analysed sample is shown in Figure 1. Mean age was 55.48 ± 6.20 years and 20 patients (69.0%) were men. Mean diabetes duration was 5.14 ± 4.44 years and mean HbA1c was 9.37 ± 1.95%, which is 2.37 percentage points above the 7% glycaemic target used in routine practice; glycaemic control is itself associated with retinal thickness in diabetic eyes.[53,54] Baseline characteristics appear in Table 1. Because the record set carries only pooled covariate summaries and not their distribution across grades, no test of whether age, duration or HbA1c differed between grades is possible, and none is reported; the bounding analysis below substitutes for it. Sex counts are internally consistent (20 + 9 = 29; 20/29 = 69.0%), and every figure quoted in this paragraph is reproduced in Table 1.

Table 1. Baseline characteristics of the study population.

Characteristic	Value	Unit of analysis
Patients	29	—
Eyes analysed	32	—
Patients contributing both eyes	3	—
Records screened before exclusions	not documented in the source	—
Age, mean ± SD (years)	55.48 ± 6.20	patient
Sex — male, n (%)	20 (69.0)	patient
Sex — female, n (%)	9 (31.0)	patient
DM duration, mean ± SD (years)	5.14 ± 4.44	patient
HbA1c, mean ± SD (%)	9.37 ± 1.95	patient
HbA1c above the 7% guideline target	+2.37 percentage points	patient
Mild NPDR, n eyes (%)	11 (34.4)	eye
Moderate NPDR, n eyes (%)	11 (34.4)	eye
Severe NPDR, n eyes (%)	10 (31.3)	eye

Demographic and metabolic variables are reported at patient level (n = 29); GCL–IPL thickness and severity grade are reported at eye level (n = 32). The record set carries only pooled covariate summaries, so their distribution across severity grades is unknown and is bounded rather than tested (Table 8). SD = standard deviation; DM = diabetes mellitus; HbA1c = glycated haemoglobin; NPDR = non-proliferative diabetic retinopathy.

Primary outcome

Mean macular GCL–IPL thickness fell monotonically across grades, as detailed in Table 2 and displayed with its confidence intervals in Figure 2: 86.0 ± 3.63 µm in mild NPDR (95% CI 83.6 to 88.4), 71.0 ± 4.71 µm in moderate NPDR (95% CI 67.8 to 74.2) and 63.8 ± 3.39 µm in severe NPDR (95% CI 61.4 to 66.2). The total spread from mild to severe was 22.2 µm, equivalent to 25.8% of the mild-grade mean. One-way analysis of variance rejected equality of means, $F(2, 29) = 86.288$, $p < 0.001$, with $\eta^2 = 0.856$ (95% CI 0.724–0.900) and $\omega^2 = 0.842$; that is, grade accounts for roughly six-sevenths of the total variance in thickness. The conclusion did not depend on the equal-variance assumption: Welch's test gave $F(2, 19.16) = 103.78$, $p < 0.001$, and the Brown–Forsythe test gave $F(2, 27.18) = 87.43$, $p < 0.001$, with a largest-to-smallest variance ratio of 1.93, comfortably inside conventional tolerance. All three omnibus tests are set out in the upper block of Table 3.

Table 2. Macular GCL–IPL thickness by NPDR severity grade, with normative benchmarking.

NPDR grade	Eyes	Mean ± SD (µm)	95% CI of the mean	Position relative to the normative floor of 72.9 µm	t	p
Mild	11	86.0 ± 3.63	83.6 to 88.4	significantly above the floor	+11.97	<0.001
Moderate	11	71.0 ± 4.71	67.8 to 74.2	CI contains the floor; not significantly below	−1.34	0.211
Severe	10	63.8 ± 3.39	61.4 to 66.2	significantly below the floor	−8.49	<0.001
All eyes	32	73.91 (grand mean)	—	—	—	—

The normative range of 72.9–92.5 µm is the one quoted in the source report and is a cross-device quotation; normative GCL–IPL values differ between OCT platforms and between ethnic groups. One-sample t tests compare each grade mean against the LOWER BOUND of that range and are benchmarking only: no healthy control group was studied, so they cannot establish that any grade is abnormal. CI = confidence interval.

Table 3. Omnibus tests and Bonferroni-adjusted pairwise contrasts.

Analysis	Statistic	df	p	Effect size (95% CI)
One-way ANOVA	F = 86.288	2, 29	<0.001	$\eta^2 = 0.856$ (0.724 to 0.900)
Welch ANOVA	F = 103.78	2, 19.16	<0.001	—
Brown–Forsythe ANOVA	F = 87.43	2, 27.18	<0.001	—
ω^2 (bias-corrected)	0.842	—	—	—
Mild vs moderate	Δ = 15.0 µm; t = 8.856	29	<0.001	g = 3.43 (2.08 to 4.78); Δ CI 10.70 to 19.30
Mild vs severe	Δ = 22.2 µm; t = 12.791	29	<0.001	g = 6.05 (3.95 to 8.16); Δ CI 17.79 to 26.61
Moderate vs severe	Δ = 7.2 µm; t = 4.148	29	0.0008	g = 1.67 (0.66 to 2.68); Δ CI 2.79 to 11.61

GRIMMER pins the within-group sums of squared deviations exactly at 132, 222 and 103.6, so the within-group mean square is exactly 457.6/29 = 15.7793 on 29 degrees of freedom and the analysis of variance can be reconstructed with no rounding allowance. Confidence intervals for mean differences are Bonferroni-adjusted across the three comparisons. Hedges' g is computed on the two grades being compared; the η^2 confidence interval comes from the non-central F distribution.

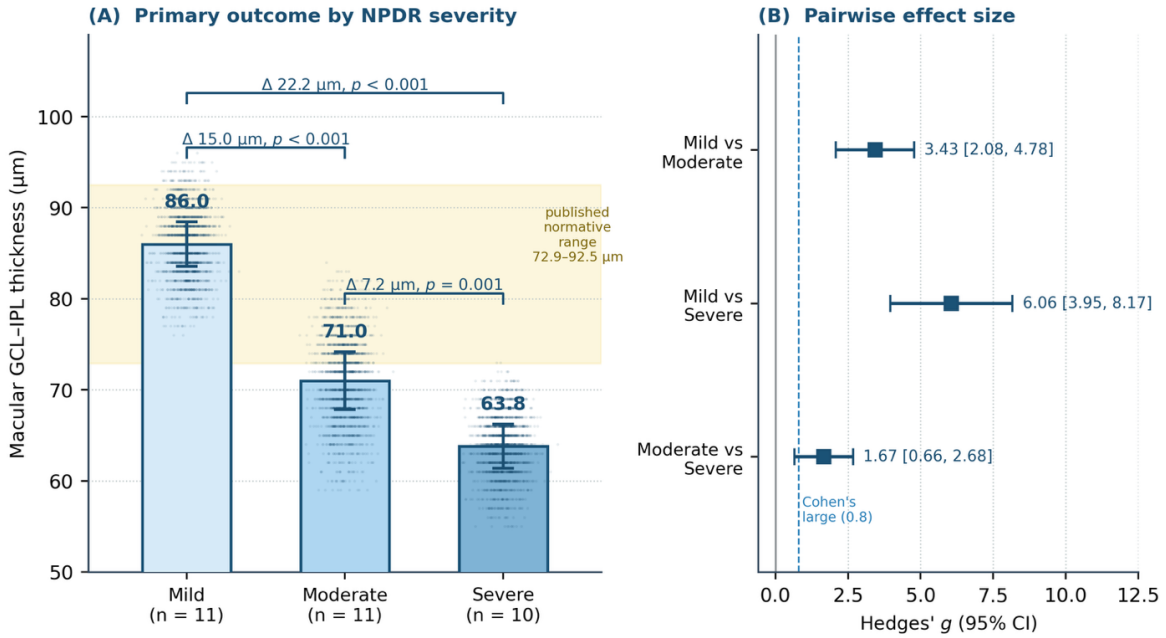

Figure 2. *Primary outcome and pairwise effect sizes. (A) Mean macular GCL–IPL thickness by NPDR grade with 95% confidence intervals. Faint points show the range of individual values across admissible eye-level reconstructions, pooled from many different reconstructions, so they illustrate the spread each grade can take rather than any single dataset. The shaded band is the normative range of 72.9–92.5 µm quoted in the source report. Brackets give the mean difference and the Bonferroni-adjusted p value. (B) Hedges' g with 95% confidence intervals; the dashed line marks Cohen's conventional threshold for a large effect.*

Pairwise contrasts

All three Bonferroni-adjusted pairwise contrasts were statistically significant, as detailed in the lower block of Table 3 and shown as effect sizes in Figure 2B. Mild exceeded moderate by 15.0 µm (95% CI 10.70 to 19.30; t(29) = 8.856, p < 0.001; Hedges' g = 3.43, 95% CI 2.08 to 4.78) and severe by 22.2 µm (95% CI 17.79 to 26.61; t(29) = 12.791, p < 0.001; g = 6.05, 95% CI 3.95 to 8.16). The moderate–severe difference was 7.2 µm (95% CI 2.79 to 11.61; t(29) = 4.148, adjusted p = 0.0008; g = 1.67, 95% CI 0.66 to 2.68). That last p value is three orders of magnitude larger than the other two, and every subsequent sensitivity analysis identifies the moderate–severe contrast as the least secure of the three; it is treated as such throughout. The source report's statement that all pairwise comparisons reached p < 0.001 is arithmetically correct, and an earlier draft of this re-analysis wrongly described it as an overstatement; that criticism is withdrawn.

Distribution of loss across grades, and its dependence on the severity scale

On an equally spaced grade score, a weighted linear fit gave a slope of −11.16 µm per grade and captured 2613.41 of the 2723.11875 between-group sum of squares, or 95.97%, tested by the correctly weighted linear contrast (t(29) = −12.870, p < 0.001). The residual one-degree-of-freedom lack-of-fit component was significant, F(1, 29) = 6.953, p = 0.013; the fit and its residuals are drawn in Figure 3A and the whole decomposition, including the lack-of-fit sum of squares of 109.71 and the 2581.54 attributable to the naive (−1, 0, 1) contrast that is often mistaken for it, is detailed in Table 4. The contrast that carries it is exactly the difference between successive decrements: the mild-to-moderate step of 15.0 µm exceeds the moderate-to-severe step of 7.2 µm by 7.8 µm (95% CI 1.75 to 13.85), a ratio of 2.08 to 1, as displayed in Figure 3B.

Table 4. Distribution of loss across grades and its dependence on the severity scale.

Component	Estimate	Test statistic	p	95% CI
Weighted linear slope, equal spacing	−11.16 µm per grade	t(29) = −12.870	<0.001	—
Linear sum of squares	2613.41, or 95.97% of the between-group SS	—	—	—
Lack of fit, equal spacing (1, 2, 3)	SS = 109.71	F(1, 29) = 6.953	0.013	—
Lack of fit, ETDRS levels (20, 43, 53)	SS = 1.51	F(1, 29) = 0.096	0.759	—
Lack of fit, alternative levels (20, 43, 47)	SS = 92.44	F(1, 29) = 5.859	0.022	—
Lack of fit, logarithmic spacing	SS = 6.90	F(1, 29) = 0.437	0.514	—
Moderate score giving an exactly linear fit	2.35 on the 1-to-3 scale	—	—	—
Lack-of-fit contrast (1, −2, 1)	+7.80 µm	t(29) = 2.637	0.013	1.75 to 13.85
Mild → moderate decrement	15.0 µm	—	—	10.70 to 19.30
Moderate → severe decrement	7.2 µm	—	—	2.79 to 11.61
Ratio of successive decrements	2.08 to 1	—	—	—

The linear component is a weighted least-squares fit of grade mean on the severity score with group sizes as weights, tested by the contrast proportional to n_g(x_g − x̄_w), which alone reproduces the regression sum of squares and is exactly orthogonal to the lack-of-fit contrast at unequal group sizes; the naive (−1, 0, 1) contrast is neither, and its sum of squares is 2581.54 against 2613.41 for the linear component. Lack-of-fit p values are unadjusted; Bonferroni correction across the four scorings gives 0.053 for the equally spaced score.

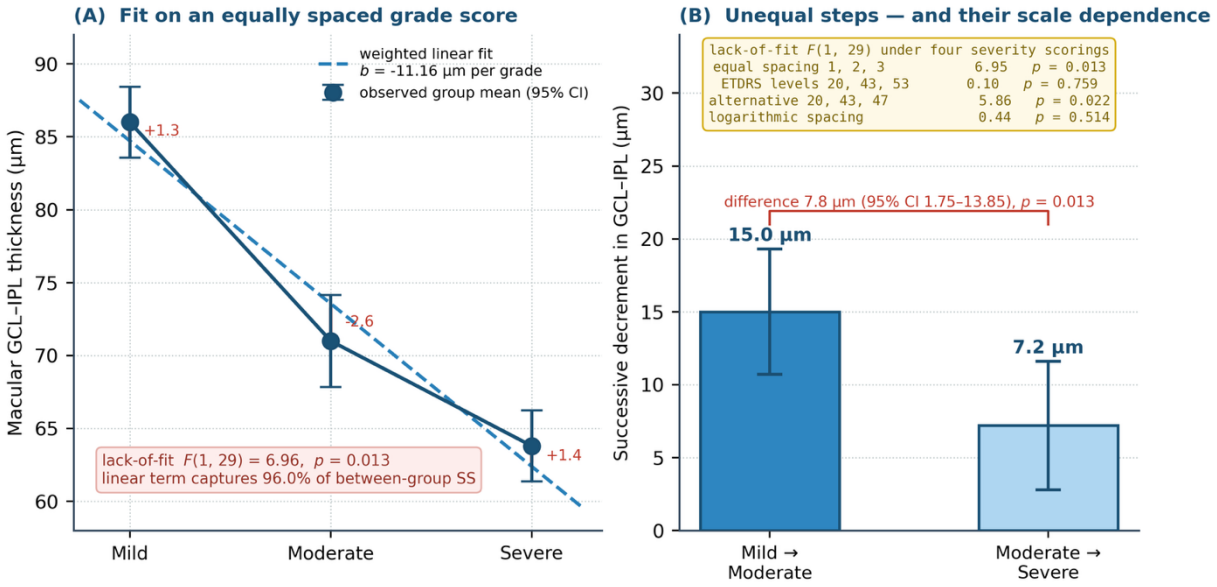

Figure 3. *Distribution of loss across grades and its dependence on the severity scale. (A) Observed grade means with 95% confidence intervals against the weighted linear fit on an equally spaced score; red segments are the residuals. (B) The two successive decrements with Bonferroni-adjusted intervals, and the lack-of-fit statistic recomputed under four severity scorings: the departure from linearity is significant on an equally spaced score and absent on the ETDRS severity levels, so it is a property of the coding rather than of the disease.*

That result is not, however, a statement about the disease until a metric for severity is fixed, and the ETDRS grades are not equally spaced on the scale from which they derive. Rescoring the three grades by their ETDRS severity levels of 20, 43 and 53 removes the departure from linearity entirely: the lack-of-fit statistic falls to F(1, 29) = 0.096, p = 0.759. Under an alternative assignment of 20, 43 and 47 it persists (F(1, 29) = 5.859, p = 0.022), and under logarithmic spacing it does not (F(1, 29) = 0.437, p = 0.514); all four scorings are listed in Table 4 and summarised in the inset of Figure 3B. A moderate-grade score of 2.35 on the 1-to-3 scale, rather than 2.00, would make the relationship exactly linear. The lack-of-fit p value is also unadjusted; carried through the same Bonferroni correction applied to the other contrasts in Table 4 it becomes 0.053. The defensible statement is therefore the descriptive one — the two clinical steps cost markedly different amounts of neuroretinal tissue, 15.0 against 7.2 µm — and not the inferential claim that neuronal loss decelerates with severity.

Rank association

Spearman's ρ between grade and thickness was −0.900 (p < 0.001, n = 32), reproducing the source analysis. That figure should be read against what is attainable rather than against unity. Searching the admissible family by coordinate ascent, the largest magnitude any compatible dataset attains is 0.9585, so the reported value is 93.9% of it; under the normality constraint the attainable maximum falls to 0.9325 and the reported value is 96.5% of that; both are detailed in the upper block of Table 5. Kendall's τ-b, which handles the heavy ties in the exposure correctly, lay between −0.826 and −0.781 across the unconstrained datasets attaining ρ = −0.900, and between −0.813 and −0.781 once normality is imposed, against a searched maximum magnitude of 0.8895. An earlier version of this analysis quoted a "tie-free ceiling" of 0.943 for ρ; that quantity assumes no ties in thickness, which inflates rather than caps the coefficient, and it was contradicted by the analysis's own sampling output. It has been replaced by the searched maximum.

Table 5. Rank association and identified discrimination bounds over the admissible datasets.

Quantity	Primary, normality imposed	Conservative, unconstrained	Status
Admissible multisets: mild / moderate / severe	960 / 4,595 / 330	1,300 / 5,738 / 441	exhaustively enumerated
Complete eye-level datasets	1,455,696,000	3,289,595,400	—
Spearman ρ, grade vs thickness	−0.900 (p < 0.001)	same	reproduces the source
Largest |ρ| attainable	0.9325; observed is 96.5% of it	0.9585; observed is 93.9% of it	search-attained maximum
Kendall τ-b given ρ = −0.900	−0.813 to −0.781	−0.826 to −0.781	identified interval
Largest |τ-b| attainable	0.8401	0.8895	search-attained maximum
U(severe > mild) of 110 pairs	0 to 0	0 to 0	fully identified
U(moderate > mild) of 121 pairs	—	0 to 7.5	sharp interval
U(severe > moderate) of 110 pairs	—	0 to 24.5	expected 11.81 under the normal model
AUC mild vs severe	1.000	1.000	arithmetic identity, not an estimate
AUC mild vs moderate	0.967 to 1.000	0.938 to 1.000	sharp interval
AUC moderate vs severe	0.827 to 0.964	0.777 to 1.000	sharp interval
Exact permutation p for AUC moderate vs severe = 0.5	—	0.024 at the least favourable admissible pair	all 352,716 splits enumerated

Sharp intervals are attained over all eye-level datasets consistent with the published means, standard deviations and counts. The primary family additionally imposes the non-significant Shapiro–Wilk result the source reports, giving 960 × 4,595 × 330 = 1,455,696,000 datasets; the unconstrained family of 1,300 × 5,738 × 441 = 3,289,595,400 is retained as a conservative alternative. Maxima for ρ and τ-b are the largest values found by coordinate ascent verified against an exhaustive sweep of each grade in turn, and are lower bounds on the true supremum. AUC = area under the receiver-operating characteristic curve.

The reported coefficient is coherent with the reported means and standard deviations. Under the normal model those summaries imply, a severe eye should be thicker than a moderate eye in 10.7% of the 110 possible pairs, giving an expected Mann–Whitney statistic of 11.81; in 200,000 simulated cohorts the mean was 11.79 (SD 7.90). Among admissible datasets attaining ρ = −0.900, that statistic ranged from 5.5 to 13.5 with a median of 11.0. There is no tension between the correlation the source reported and the descriptive statistics reported alongside it.

Discrimination and a candidate threshold

Because the ordering within grades is not identified by the published summaries, discrimination is reported as a sharp interval over the admissible family, detailed in the lower block of Table 5 and drawn as receiver-operating envelopes in Figure 4A. Mild and severe eyes were completely separated in every dataset: the smallest value any admissible mild multiset can contain is 76 µm and the largest any severe multiset can contain is 73 µm, so the Mann–Whitney statistic is identically zero and the area under the curve is exactly 1.000 as a matter of arithmetic rather than of estimation. Mild versus moderate gave 0.967–1.000 under the normality constraint (0.938–1.000 without it). Moderate versus severe — the only genuinely overlapping pair — gave 0.827–0.964 under the constraint and 0.777–1.000 without it. Exact permutation over all 352,716 splits, evaluated at the least favourable admissible pair, gives a two-sided p of 0.024; that is the correct worst case, and an earlier statement that the permutation p never exceeded 0.006 was based on a sample of reconstructions rather than the extremum and was wrong.

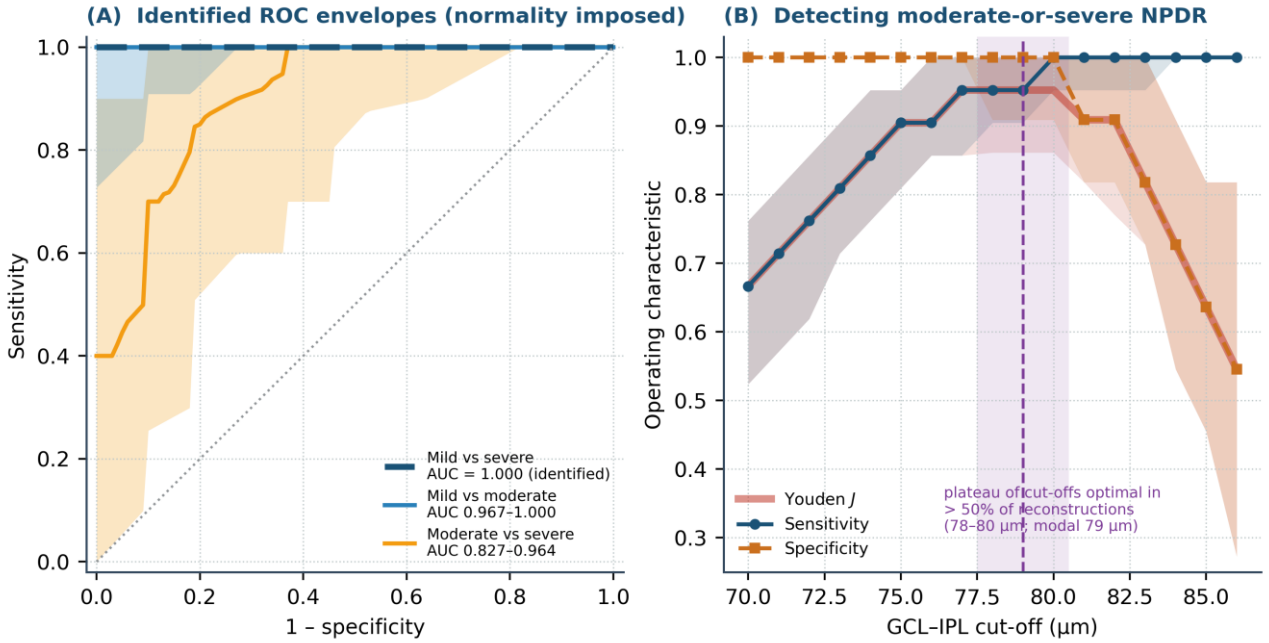

Figure 4. *Discrimination and threshold selection. (A) Receiver-operating characteristic envelopes; each shaded region spans every curve attainable across admissible eye-level datasets under the normality constraint, and the line is the median. Mild and severe eyes cannot overlap in any admissible dataset (dashed navy). (B) Sensitivity, specificity and the Youden index for detecting moderate-or-severe NPDR as a function of the cut-off; shaded bands are the 2.5th to 97.5th percentile across reconstructions, and the shaded panel marks the plateau of cut-offs optimal in more than half of them.*

Treating moderate-or-severe NPDR as the target condition, the Youden-optimal cut-off is not a single value but a plateau, as detailed in Table 6 and traced across the whole cut-off range in Figure 4B. Across reconstructions the maximising cut-off ranged from 71 to 86 µm; three values — 78, 79 and 80 µm — were optimal in more than half of them, with 79 µm the most frequent at 64.8%. At 79 µm, median sensitivity was 0.952 (identification range 0.905–1.000; Wilson 95% CI 0.773–0.992) and median specificity 1.000 (range 0.909–1.000; Wilson 95% CI 0.741–1.000). Because each column of Table 6 is a separate median across reconstructions, the tabulated sensitivity, specificity and Youden index in a given row need not satisfy the identity J = Se + Sp − 1; the Youden column is the median of the index itself. All of these figures are derived in the same small cohort that generated them and are optimistically biased. The operating characteristics quoted here are the same values tabulated in the third row of Table 6.

Table 6. Operating characteristics of candidate GCL–IPL thresholds for moderate-or-severe NPDR.

Cut-off	Optimal share	Sensitivity, median (range)	Sensitivity Wilson 95% CI	Specificity, median (range)	Specificity Wilson 95% CI	Youden J
< 77 µm	35.4%	0.952 (0.857–1.000)	0.773 to 0.992	1.000 (0.909–1.000)	0.741 to 1.000	0.952
< 78 µm	53.7%	0.952 (0.857–1.000)	0.773 to 0.992	1.000 (0.909–1.000)	0.741 to 1.000	0.952
< 79 µm	64.8%	0.952 (0.905–1.000)	0.773 to 0.992	1.000 (0.909–1.000)	0.741 to 1.000	0.952
< 80 µm	62.0%	1.000 (0.905–1.000)	0.845 to 1.000	1.000 (0.818–1.000)	0.741 to 1.000	0.952
< 81 µm	43.8%	1.000 (0.952–1.000)	0.845 to 1.000	0.909 (0.818–1.000)	0.623 to 0.984	0.909

Target condition is moderate or severe NPDR (21 eyes) against mild NPDR (11 eyes). Ranges are the identification spread across admissible datasets; Wilson intervals express sampling uncertainty at the median counts. Each column is a SEPARATE median across reconstructions, so a row need not satisfy the identity J = Se + Sp − 1; the last column is the median of the Youden index itself. "Optimal share" is the proportion of reconstructions in which that cut-off attains the maximum Youden index, counting ties. The maximising cut-off ranged from 71 to 86 µm across the family. All figures are in-sample and optimistically biased; no external validation has been performed.

Sensitivity analyses

Intra-patient clustering had a modest effect. With Kish's effective cluster size of 1.1875, the design effect reaches 1.178 at an intraclass correlation of 0.95, reducing the effective sample size from 32 to 27.2 eyes; deflating F by the design effect gives F = 73.24 on (2, 24.2) degrees of freedom, $p = 5.5 \times 10^{-11}$, as detailed in the first row of Table 7. Worst-case confounding was bounded by constrained optimisation, with the closed-form solution used to verify the numerical optimum and the constraint confirmed active. Even if the entire reported variance of each covariate were concentrated between grades and aligned in the same direction, age could account for at most 3.77 µm of the 22.2 µm mild–severe gap, diabetes duration for 3.24 µm and HbA1c for 2.37 µm, a combined maximum of 9.38 µm or 42.3%. At least 12.82 µm of that gap is therefore identified as not attributable to those three covariates.

Table 7. Sensitivity analyses: clustering, worst-case confounding, E-values and detectable effects.

Analysis	Result	Interpretation
Design effect at ICC 0.95, Kish	DEFF 1.178; effective n 27.2 eyes	F deflated to 73.24 on (2, 24.2), $p = 5.5 \times 10^{-11}$
Maximum confounding by age, mild vs severe	3.77 µm, or 17.0% of 22.2 µm	at 100% between-grade variance
Maximum confounding by DM duration, mild vs severe	3.24 µm, or 14.6%	at 100% between-grade variance
Maximum confounding by HbA1c, mild vs severe	2.37 µm, or 10.7%	at 100% between-grade variance
Combined worst case, mild vs severe	9.38 µm against 22.2 µm observed	at least 12.82 µm identified as unconfounded; PROTECTED
Combined worst case, moderate vs severe	9.38 µm against 7.2 µm observed	critical variance fraction 0.589; NOT protected
Combined worst case, lack-of-fit contrast	15.99 µm against 7.8 µm observed	critical variance fraction 0.238; the LEAST protected result in the paper
E-value, mild vs severe	619.8; 84.83 at the 95% limit; 54.50 at the Bonferroni limit	point value outside the calibrated range of the approximation
E-value, mild vs moderate	50.8; 14.02 at the 95% limit; 10.47 at the Bonferroni limit	not explicable by confounding
E-value, moderate vs severe	9.2; 3.26 at the 95% limit; 2.51 at the Bonferroni limit	substantial but of a lower order
Detectable effect, omnibus, 80% power	Cohen's f = 0.578, or $\eta^2 = 0.251$	study powered only for large effects
Detectable difference, moderate vs severe	5.89 µm, Bonferroni-adjusted	the observed 7.2 µm sits just above it
Eyes per grade for ± 2 µm precision	33	target for a confirmatory study

Cluster sizes are unequal, being 26 singletons and 3 pairs, so the design effect uses Kish's effective cluster size of 1.1875 rather than the naive mean of 1.1034, and F is deflated by it. Confounding bounds maximise each contrast subject to the covariate's reported total sum of squares; the closed-form solution was used to verify the numerical optimum and the constraint was confirmed active. External slope estimates: −0.25 µm per year of age, −0.30 µm per year of diabetes, −0.50 µm per percentage point of HbA1c. Summing the three worst cases is conservative and assumes they can be extreme simultaneously. E-values follow VanderWeele and Ding; a standardised difference above about 3 lies outside the calibrated range of the approximation.

The same envelope does not protect the other two contrasts, and this is the most important qualification in the paper. For moderate versus severe, 58.9% of each covariate's total variance would have to lie between those two grades, all three aligned, to erase a 7.2 µm difference. For the lack-of-fit contrast the worst case is 15.99 µm against an observed 7.8 µm, so only 23.8% of each covariate's variance need be so distributed. The unequal-decrement finding is thus the least protected result in this analysis, not the most — a conclusion that points the same way as its scale-dependence and its unadjusted p value.

E-values were computed at three levels of stringency, as detailed in the lower block of Table 8. For mild versus severe the point-estimate E-value is 619.8, but a standardised mean difference of 6.30 lies far outside the range in which the approximation used to convert it to a risk ratio is calibrated, so the limit values are the meaningful ones: 84.83 at the 95% limit and 54.50 at the Bonferroni-consistent limit. For mild versus moderate the corresponding limit values are 14.02 and 10.47. For moderate versus severe they fall to 3.26 and 2.51, which is still more than a trivial confounder could supply but is of a different order, and is consistent with every other line of evidence identifying that contrast as the weakest in the set.

4. Discussion

In 32 eyes of 29 adults attending the vitreoretinal service of Dr. M. Djamil General Hospital, Padang, mean macular GCL–IPL thickness fell steeply and monotonically across ETDRS NPDR grades, with grade accounting for 85.6% of the variance in thickness. Descriptively, the two clinical steps cost very different amounts of tissue: 15.0 µm from mild to moderate against 7.2 µm from moderate to severe. What this study also shows, and what distinguishes it from the correlation-based literature, is how little of that asymmetry survives scrutiny as an inferential claim.

The lack-of-fit test that makes the asymmetry statistically significant is defined relative to a numerical score for the grades. On the equally spaced score that clinicians implicitly use when they say "one grade worse", the departure from linearity is real (p = 0.013). On the ETDRS severity levels from which the grades derive, it vanishes (p = 0.759). A moderate-grade score of 2.35 rather than 2.00 would make the relationship exactly linear, and the ETDRS levels place moderate at 43 on a 20-to-53 interval, which is 0.70 of the way — close to that value. In other words, the data are equally consistent with a strictly linear decline in a severity metric on which moderate NPDR is closer to severe than to mild, which is precisely what the ETDRS scale asserts.[45,46] Because the Bonferroni-corrected lack-of-fit p is 0.053 and the contrast is the least protected of all against confounding, the honest conclusion is that this study cannot determine the shape of the relationship, only its steepness. Reporting it any other way would let an arbitrary coding decision masquerade as a biological finding.

That said, the descriptive fact has clinical content independent of any curve. Clinicians act on grades, not on ETDRS levels: a patient is told they have moved from mild to moderate retinopathy. Whatever the underlying metric, the transition that clinicians observe first coincides with the larger loss of neuroretinal tissue, and this is where a structural marker carries most information. It is also the transition at which trials of neuroprotection would have most room to act, since neuroprotection presupposes neural tissue that has not yet been lost,[18] and staging proposals that incorporate neural change point the same way.[14,15] A trial enrolling severe NPDR would be enrolling eyes in which the structural endpoint has largely already moved. The same logic bears on prognostic modelling: deep-learning systems that predict time to progression are trained predominantly on vascular features,[7] so a neuronal marker that saturates early would carry information those models do not currently exploit.[15]

Placing the present estimates alongside published series is instructive. Cross-sectional studies contrasting diabetes without retinopathy against healthy controls typically report differences of a few micrometres,[19,21,23,57] and predictive analyses of pre-clinical neurodegeneration report effects of similar magnitude.[30] The 15.0 µm mild-to-moderate decrement observed here is several times larger, and the comparison is worth making carefully. Series that grade the neuronal measurement by retinopathy severity rather than by its presence report gradients in the same direction but of smaller amplitude,[31,32,35] and the mild-to-moderate step reported here exceeds them. Longitudinal work also shows how slowly this compartment normally changes: annual loss in eyes followed over two to five years is measured in small fractions of a micrometre,[58-61] which makes a 15.0 µm difference between adjacent grades a large quantity of tissue however it accrued. Two explanations are plausible and not mutually exclusive. Referral to a provincial tertiary vitreoretinal clinic selects for eyes at the more advanced end of each grade, which would widen every between-grade contrast. The cohort's mean HbA1c of 9.37% is also far above that of most published European and East Asian series; that comparison is worth making, but it cannot be a quantitative explanation of the gap, since even the maximal between-grade HbA1c imbalance this dataset permits accounts for only 2.37 µm. Vrabec and colleagues, studying NPDR without macular oedema, likewise found GCL–IPL linked to both HbA1c and diabetes duration,[25] and systemic determinants including renal function track inner-retinal thickness independently;[62,63] structure–function work using microperimetry points the same way.[43,64] Retinal arterial morphometry,[65] choroidal change[66] and even tobacco exposure[67] have each been shown to move the same compartment, which is a further reason to read an unadjusted between-grade difference as an upper bound on the disease effect.

The discrimination results are more robust than either the correlation or the shape analysis. A Spearman coefficient of −0.900 sounds close to perfect, but the largest magnitude any dataset compatible with these summaries can attain is 0.9585, so the observed figure is 93.9% of what is reachable. What the data do establish beyond dispute is separation. The smallest value an admissible mild multiset can contain exceeds the largest an admissible severe multiset can contain, so mild and severe eyes cannot overlap in any dataset consistent with the published means and standard deviations; the area under the curve for that contrast is a theorem, not an estimate. Moderate versus severe remains genuinely uncertain, at 0.827–0.964 with the source's own normality result imposed and 0.777–1.000 without it, with a worst-case exact permutation p of 0.024.

The candidate threshold near 79 µm for detecting moderate-or-severe NPDR is offered as a hypothesis for prospective testing and emphatically not as a rule. It was derived within the same small cohort that generated it and is optimistically biased; the maximising cut-off ranged from 71 to 86 µm across reconstructions, and its Wilson intervals, 0.773–0.992 for sensitivity and 0.741–1.000 for specificity, are wide because the denominators are 21 and 11 eyes. A sensitivity whose lower confidence limit is 0.773 means that up to roughly one eye in four with moderate or severe disease could be missed, so the threshold must never be used to lengthen a review interval that fundoscopic grading would shorten. The mechanism, and a pathway in which such a measurement sits alongside and strictly subordinate to ETDRS grading and the review intervals that guidelines already specify, are set out in Figure 5.[45,46]

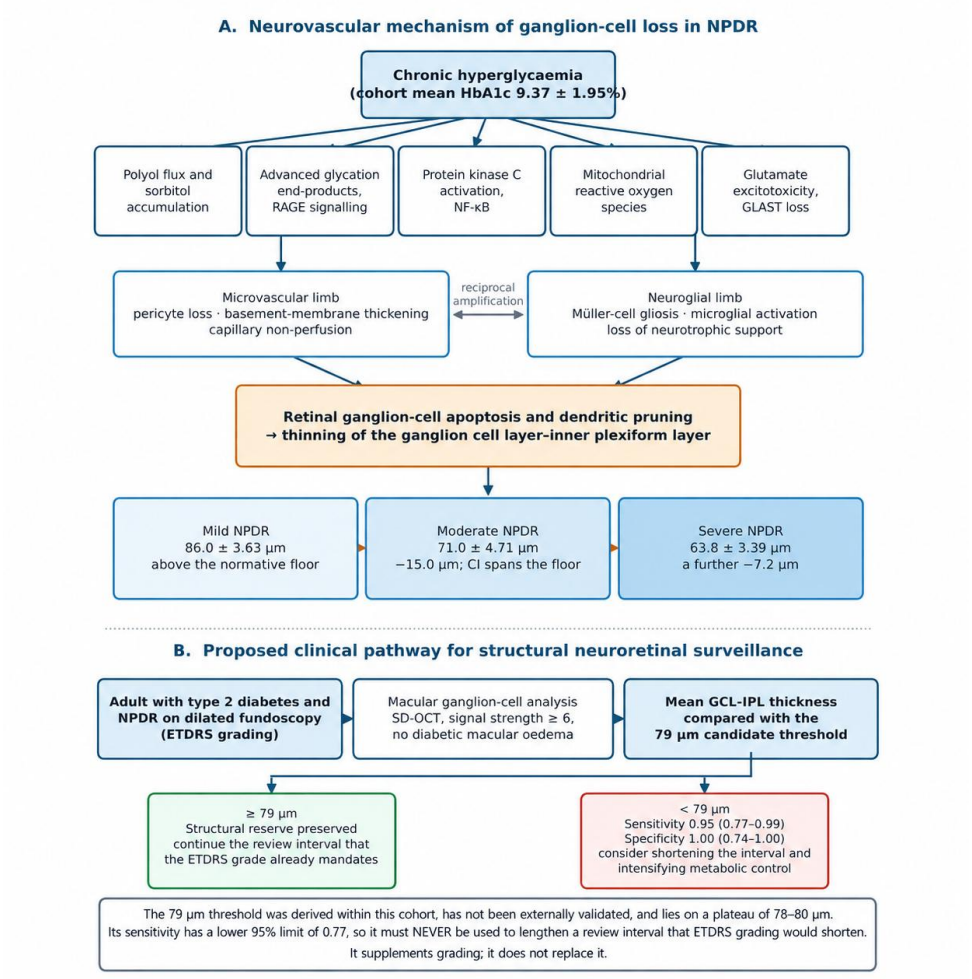

Figure 5. *Mechanism and proposed clinical pathway. (A) Hyperglycaemia-driven pathways converge on the microvascular and neuroglial limbs of the retinal neurovascular unit, which amplify one another and together produce ganglion-cell loss; the observed decrements between grades are shown below. (B) A pathway in which a macular ganglion-cell analysis obtained at the same sitting as routine macular OCT supplements, and never overrides, ETDRS grading. The threshold is a hypothesis for prospective validation and must not be used to lengthen a review interval that grading would shorten.*

For Indonesian practice the implications are practical rather than aspirational. Diagnostic capacity for diabetic eye disease is unevenly distributed across the archipelago and concentrated in provincial referral hospitals such as Dr. M. Djamil,[3,4] and the screening models proposed for middle-income systems rely on making each patient contact yield more information.[5,68] Macular OCT is already performed on patients referred to Indonesian tertiary eye services for suspected maculopathy, so extracting a ganglion-cell analysis at the same sitting adds seconds rather than a new investigation. The Indonesian national standard already mandates annual retinal examination in type 2 diabetes, yet community-based screening still finds substantial undetected retinopathy at first contact,[69] and both the American Diabetes Association and the American Academy of Ophthalmology stratify the review interval by severity grade.[70,71] An objective, quantitative structural marker would complement grading in exactly the settings where inter-observer agreement on the 4-2-1 rule is hardest to maintain — the more so here, where grading rested on a single consultant and no agreement statistic exists.

The strengths of this analysis are threefold. Every statistic in the source report was recomputed and reproduced exactly, and the analysis-of-variance table was shown to be internally exact rather than merely approximately consistent. Because record-level data were unavailable, no single reconstruction was assumed; instead every dataset compatible with the published summaries — and, in the primary analysis, with the source's own normality result — was enumerated, so each quantity is reported either as identified or as a sharp interval, and no result depends on an unverifiable choice. And the robustness of each finding was quantified separately rather than asserted collectively, which is what allowed this analysis to establish that its most striking descriptive result is also its most fragile inferential one.

The limitations are correspondingly clear. The design is cross-sectional and retrospective, so no causal or temporal claim is warranted; the unequal decrements are differences between grades at one moment, not observed trajectories within eyes, and only a longitudinal cohort can establish the latter. There is no healthy control group, which is why the claim of pre-clinical thinning has been withdrawn. Grading rested on a single consultant with no second reader, so no reliability estimate is available, and misgrading would attenuate the very contrasts reported here. The number of records screened before exclusion was not documented, so selection cannot be characterised. The sample of 32 eyes from a single tertiary centre is small and selected: it was powered only for large effects (η^2 of at least 0.251), the moderate–severe contrast has an adjusted p of 0.0008 with a confounding bound that does not protect it, and generalisation beyond poorly controlled, tertiary-referred West Sumatran patients is not supported. Axial length, refractive error, blood pressure, renal function and treatment history were not recorded, all of which influence inner-retinal thickness and none of which could be bounded here. Neither the OCT device model nor the segmentation software version was documented, which limits transfer of any absolute threshold to other platforms, the more so because GCL–IPL values are not interchangeable between spectral-domain and swept-source instruments.[56] Two further determinants of GCL–IPL thickness could not be excluded: myopia and axial length reduce measured GCL–IPL independently of any retinal disease,[55,72] and refraction was not recorded, so a differential distribution of myopia across grades cannot be ruled out; and glaucoma and glaucoma suspicion produce the same pattern of macular GCL–IPL loss reported here and are in fact diagnosed by it,[73] yet no formal glaucoma exclusion is documented in the record set. Finally, every digital object identifier in the bibliography was resolved against Crossref and each record's authors, title, journal and year were taken from the resolved record rather than from recall, but no independent reading of every full text was possible.

5. Conclusion

Macular GCL–IPL thickness declines steeply across NPDR severity in this Indonesian tertiary cohort, accounting for 85.6% of the variance in thickness, and the two clinical steps cost markedly different amounts of tissue: 15.0 µm from mild to moderate against 7.2 µm from moderate to severe. That asymmetry should be read descriptively and not as evidence that neuronal loss decelerates, because it is a property of the equally spaced grade score and disappears when the grades are scored by their ETDRS levels. The mild-grade mean remained within the published normative band and the moderate grade's interval contains the normative floor, so these data demonstrate a severity gradient rather than pre-clinical thinning — a reference interval built for individual eyes cannot be used to certify a group mean as normal, and the corresponding claim in the original report is withdrawn. Mild and severe eyes are completely separated on GCL–IPL in every dataset compatible with the published summaries. A threshold near 79 µm identified moderate-or-severe disease with high sensitivity and specificity, but within-sample derivation and a wide confidence interval make it a hypothesis rather than a rule, and it must not be used to lengthen any review interval. Prospective, longitudinal, multicentre work with a healthy control arm, two graders, recorded axial length and a stated OCT platform is required to establish the shape of the relationship, to validate the threshold externally, and to test whether the mild-to-moderate transition is the window in which neuroprotection can still act.

Declarations

Ethical approval. This study received ethical approval from CMHC Research Center, Indonesia (Ref No CMHC/VI/2023/099).

Availability of data and materials. The complete analysis code, including the enumeration of admissible eye-level datasets, the constrained-optimisation confounding bounds and the figure-generation scripts, is available from the corresponding author on reasonable request. Record-level clinical data cannot be shared because consent for redistribution was not obtained.

Conflict of interest. The authors declare that they have no competing interests.

Funding. This research received no specific grant from any funding agency in the public, commercial or not-for-profit sectors.

Author contributions. SYR conceived the study, extracted and curated the clinical data, and drafted the manuscript. WH and KR supervised the vitreoretinal grading, contributed to interpretation and revised the manuscript critically for important intellectual content. All authors have reviewed and approved the final version of the manuscript and agree to be accountable for all aspects of the work.

Use of artificial intelligence. The authors declare that no generative artificial intelligence tools were used in the design, analysis, or writing of this manuscript. The authors take full responsibility for the scientific content and for every interpretation presented.

Acknowledgements. The authors thank the staff of the Ophthalmology Clinic of Dr. M. Djamil General Hospital, Padang, for maintaining the imaging records on which this analysis depends.

6. References

1. Teo ZL, Tham YC, Yu M, et al. Global Prevalence of Diabetic Retinopathy and Projection of Burden through 2045. Ophthalmology 2021;128(11):1580-1591. doi:10.1016/j.ophtha.2021.04.027
2. Meng Y, Liu Y, Ma Y, et al. Global, Regional, and National Burden of Blindness due to Diabetic Retinopathy, 1990-2021. Ophthalmology and Therapy 2025;14(10):2599-2615. doi:10.1007/s40123-025-01230-y
3. Oktora SI, Butar Butar D. Determinants of Diabetes Mellitus Prevalence in Indonesia. Jurnal Kesehatan Masyarakat 2022;18(2):266-273. doi:10.15294/kemas.v18i2.31880

4. Nuridzin DZ, Aghram N, Mawarni A, et al. Determinants of Diabetes Mellitus Prevalence in Indonesia: a Multiple Linear Regression Model in an Ecological Analysis of Adults Aged 15 Years and Older. Jurnal Manajemen Kesehatan Indonesia 2024;12(3):327-338. doi:10.14710/jmki.12.3.2024.327-338
5. Thapa R, Sharma S, Pradhan E, et al. Prevalence and associated factors of diabetic retinopathy among people with diabetes screened using fundus photography at a community diabetic retinopathy screening program in Nepal. BMC Ophthalmology 2023;23(1). doi:10.1186/s12886-023-03173-z
6. Zhang G, Chen W, Chen H, et al. Risk factors for diabetic retinopathy, diabetic macular edema, and sight-threatening diabetic retinopathy. Asia-Pacific Journal of Ophthalmology 2024;13(3):100067. doi:10.1016/j.apjo.2024.100067
7. Dai L, Sheng B, Chen T, et al. A deep learning system for predicting time to progression of diabetic retinopathy. Nature Medicine 2024;30(2):584-594. doi:10.1038/s41591-023-02702-z
8. Qiu AW, Huang DR, Li B, et al. IL-17A injury to retinal ganglion cells is mediated by retinal Müller cells in diabetic retinopathy. Cell Death & Disease 2021;12(11). doi:10.1038/s41419-021-04350-y
9. Liu C, Dong W, Lv Z, et al. Thioredoxin-interacting protein in diabetic retinal neurodegeneration: A novel potential therapeutic target for diabetic retinopathy. Frontiers in Neuroscience 2022;16. doi:10.3389/fnins.2022.957667
10. Shi R, Chen L, Wang W, et al. Plasma miR-26a-5p is a biomarker for retinal neurodegeneration of early diabetic retinopathy. Eye 2021;35(6):1587-1599. doi:10.1038/s41433-021-01393-5
11. Madrakhimov SB, Yang JY, Kim JH, et al. mTOR-dependent dysregulation of autophagy contributes to the retinal ganglion cell loss in streptozotocin-induced diabetic retinopathy. Cell Communication and Signaling 2021;19(1). doi:10.1186/s12964-020-00698-4
12. Liu J, Yu H, Yu S, et al. GLCCI1 alleviates GRP78-initiated endoplasmic reticulum stress-induced apoptosis of retinal ganglion cells in diabetic retinopathy by upregulating and interacting with HSP90AB1. Scientific Reports 2024;14(1). doi:10.1038/s41598-024-75874-4
13. Zhang Y, Li T, Cai X, et al. Sirt5-mediated desuccinylation of OPTN protects retinal ganglion cells from autophagic flux blockade in diabetic retinopathy. Cell Death Discovery 2022;8(1). doi:10.1038/s41420-022-00861-5
14. Tang Z, Yang D, Nguyen TX, et al. Relationship of OCT-Based Diabetic Retinal Neurodegeneration to the Development and Progression of Diabetic Retinopathy: A Cohort Study. Investigative Ophthalmology & Visual Science 2025;66(2):32. doi:10.1167/iovs.66.2.32
15. Kim K, Kim ES, Yu SY. Prediction of Diabetic Retinopathy Severity Using a Combination of Retinal Neurodegeneration and Capillary Nonperfusion on Optical Coherence Tomography Angiography. Retina 2023;43(8):1291-1300. doi:10.1097/iae.0000000000003820
16. Xu X, Xiao H, Lai K, et al. Determinants of macular ganglion cell-inner plexiform layer thickness in normal Chinese adults. BMC Ophthalmology 2021;21(1). doi:10.1186/s12886-021-02023-0
17. Tong J, Phu J, Alonso-Caneiro D, et al. High sampling resolution optical coherence tomography reveals potential concurrent reductions in ganglion cell-inner plexiform and inner nuclear layer thickness but not in outer retinal thickness in glaucoma. Ophthalmic and Physiological Optics 2022;43(1):46-63. doi:10.1111/opo.13065
18. Zerbini G, Maestroni S, Viganò I, et al. Progressive Thinning of Retinal Nerve Fiber Layer/Ganglion Cell Layer (RNFL/GCL) as Biomarker and Pharmacological Target of Diabetic Retinopathy. International Journal of Molecular Sciences 2023;24(16):12672. doi:10.3390/ijms241612672
19. Bala B, Biswas S, Banerjee C. Retinal Neurodegeneration in Preclinical Diabetic Retinopathy: Structural Evidence from Optical Coherence Tomography. Acta Medica International 2026;13(1):558-562. doi:10.21276/amit.2026.v13.i1.391
20. Ku JY, Knox PC, Czanner G, et al. Functional and structural biomarkers linked to diabetic retinal neurodegeneration in pre-clinical and early diabetic retinopathy. BMC Ophthalmology 2025;26(1). doi:10.1186/s12886-025-04564-0
21. Lee MW, Lee WH, Ryu CK, et al. Peripapillary Retinal Nerve Fiber Layer and Microvasculature in Prolonged Type 2 Diabetes Patients Without Clinical Diabetic Retinopathy. Investigative Opthalmology & Visual Science 2021;62(2):9. doi:10.1167/iovs.62.2.9
22. Lee MW, Lim HB, Kim MS, et al. Effects of prolonged type 2 diabetes on changes in peripapillary retinal nerve fiber layer thickness in diabetic eyes without clinical diabetic retinopathy. Scientific Reports 2021;11(1). doi:10.1038/s41598-021-86306-y
23. Ambiya V, Kumar A, Bhavaraj VR, et al. Study of inner retinal neurodegeneration in Diabetes Mellitus using spectral domain optical coherence tomography. European Journal of Ophthalmology 2021;32(5):3074-3081. doi:10.1177/11206721211048793
24. Chai Q, Yao Y, Guo C, et al. Structural and functional retinal changes in patients with type 2 diabetes without diabetic retinopathy. Annals of Medicine 2022;54(1):1816-1825. doi:10.1080/07853890.2022.2095010
25. Vrabec R, Bulum T, Ljubić S, et al. Association Between Macular Ganglion Cell-Inner Plexiform Layer and Non-Proliferative Retinopathy Without Macular Edema in Type 2 Diabetes via Diabetes Duration and HbA1c Link. Biomedicines 2025;13(2):398. doi:10.3390/biomedicines13020398
26. Cetin EN, Parca O, Akkaya HS, et al. Association of inner retinal reflectivity with qualitative and quantitative changes in retinal layers over time in diabetic eyes without retinopathy. Eye 2021;36(6):1253-1260. doi:10.1038/s41433-021-01607-w
27. Seo JS, Cho YW, Seo SW, et al. Microvasculature and Nerve Fiber Layer-Ganglion Cell Inner Plexiform Layer Thickness in Type 2 Diabetes. Journal of the Korean Ophthalmological Society 2021;62(6):769-776. doi:10.3341/jkos.2021.62.6.769
28. Bhattarai S, Lavaju P, Badhu BP, et al. Retinal Nerve Fiber Layer and Macular Thickness in Patients with Type 2 Diabetes Mellitus without Retinopathy Using Optical Coherence Tomography: A Comparative Study. Nepalese Journal of Ophthalmology 2023;15(1):14-23. doi:10.3126/nepjoph.v15i1.47629
29. Ezhilvendhan K, Shenoy A, Rajeshkannan R, et al. Evaluation of Macular Thickness, Retinal Nerve Fiber Layer and Ganglion Cell Layer Thickness in Patients among Type 2 Diabetes Mellitus Using Optical Coherence Tomography. Journal of Pharmacy and Bioallied Sciences 2021;13(Suppl 2):S1055-S1061. doi:10.4103/jpbs.jpbs_165_21
30. Sooryanarayana SP, Hairol MI. Sociodemography, diabetes mellitus clinical parameters, and retinal morphology as predictors of neurodegeneration in preclinical diabetic retinopathy. Saudi Journal of Ophthalmology 2024;40(1):57-65. doi:10.4103/sjopt.sjopt_42_24
31. Sung JY, Lee MW, Lim HB, et al. The Ganglion Cell-Inner Plexiform Layer Thickness/Vessel Density of Superficial Vascular Plexus Ratio According to the Progression of Diabetic Retinopathy. Investigative Opthalmology & Visual Science 2022;63(6):4. doi:10.1167/iovs.63.6.4
32. Kaushal N, Guliani NC, Guliani BP. Profile of Macular Ganglion Cell-inner Plexiform Layer Thickness in Diabetics With and Without Retinopathy. Delhi Journal of Ophthalmology 2024;34(1):27-31. doi:10.4103/dljo.dljo_183_23
33. Pemp B, Palkovits S, Sacu S, et al. Associations of retinal neurovascular dysfunction with inner retinal layer thickness in non-proliferative diabetic retinopathy. Graefe's Archive for Clinical and Experimental Ophthalmology 2024;262(12):3761-3771. doi:10.1007/s00417-024-06552-4
34. Wu J. Dyslipidemia and reduced retinal layer thicknesses in mild to moderate non-proliferative diabetic retinopathy. American Journal of Translational Research 2024;16(10):5718-5727. doi:10.62347/ehtp6496
35. Lee MW, Kim JT, Seong HJ, et al. Peripapillary microvasculature and retinal nerve fiber layer damage according to the severity of diabetic retinopathy. Acta Diabetologica 2024;61(10):1293-1300. doi:10.1007/s00592-024-02308-y
36. Wang S, Wang Y, Li D, et al. Temporal Sector Thickening of the Retinal Nerve Fiber Layer as a Structural Marker of Diabetic Retinopathy Severity in Chinese Adults with Type 2 Diabetes Mellitus. Retina 2026. doi:10.1097/iae.0000000000004969
37. Ulhaq ZS, Hasan YTN, Herawangsa S, et al. The retinal nerve fiber layer thickness is useful for the assessment of diabetic retinopathy severity. Diabetes Epidemiology and Management 2022;7:100075. doi:10.1016/j.deman.2022.100075
38. Nadia FA. The Relationship Between Diabetic Retinopathy Degree With Visual Acuity And Retinal Nerve Fiber Layer Thickness In Type 2 Diabetes Mellitus Patients. Sumatera Medical Journal 2022;5(3). doi:10.32734/sumej.v5i3.9190
39. Nadia FA, Sari MD, Delfi. Diabetes Duration and Retinal Nerve Fiber Layer Thickness Related Degree of Diabetic Retinopathy. Ophthalmologica Indonesiana 2024;49(S2). doi:10.35749/857sg474
40. Bansal K, Mittal T, Aggarwal R. Evaluation of Peripapillary Retinal Nerve Fiber Layer and Macular Ganglion Cell-Inner Plexiform Layer Thickness in Type 2 Diabetes Mellitus Using Spectral-Domain Optical Coherence Tomography. International Journal For Multidisciplinary Research 2025;7(6). doi:10.36948/ijfmr.2025.v07i06.59091
41. Gong X, Wang W, Xiong K, et al. Associations Between Peripapillary Retinal Nerve Fiber Layer and Choroidal Thickness With the Development and Progression of Diabetic Retinopathy. Investigative Opthalmology & Visual Science 2022;63(2):7. doi:10.1167/iovs.63.2.7
42. Srinivasan S, Sivaprasad S, Rajalakshmi R, et al. Early retinal functional alteration in relation to diabetes duration in patients with

type 2 diabetes without diabetic retinopathy. Scientific Reports 2022;12(1). doi:10.1038/s41598-022-15425-x
43. Pandurangan K, Sachidanandam R, Sen P. Structural and functional changes among diabetics with no diabetic retinopathy and mild non-proliferative diabetic retinopathy using swept-source optical coherence tomography angiography and photopic negative response. Documenta Ophthalmologica 2022;145(2):113-125. doi:10.1007/s10633-022-09891-x
44. von Elm E, Altman DG, Egger M, et al. The Strengthening the Reporting of Observational Studies in Epidemiology (STROBE) statement: guidelines for reporting observational studies. The Lancet 2007;370(9596):1453-1457. doi:10.1016/s0140-6736(07)61602-x
45. Early Treatment Diabetic Retinopathy Study Research Group. Grading Diabetic Retinopathy from Stereoscopic Color Fundus Photographs-An Extension of the Modified Airlie House Classification. Ophthalmology 1991;98(5):786-806. doi:10.1016/s0161-6420(13)38012-9
46. Wilkinson CP, Ferris FL, Klein RE, et al. Proposed international clinical diabetic retinopathy and diabetic macular edema disease severity scales. Ophthalmology 2003;110(9):1677-1682. doi:10.1016/s0161-6420(03)00475-5
47. Sukmawati N, Suryathi NMA, Andayani A, et al. Differences of Retinal Nerve Fiber Layer and Ganglion Cell Layer-Inner Plexiform Layer Thickness in Patients without Diabetes Mellitus, with Diabetes Mellitus Type 2 without Diabetic Retinopathy and with Diabetic Retinopathy. International Journal of Retina 2025;8(1):1. doi:10.35479/ijretina.2025.vol008.iss001.314
48. Verma S, Singh VK, Rana J, et al. Quantitative measurement of retinal nerve fiber layer thickness and its correlation with optical coherence tomography angiography vascular biomarker changes in preclinical diabetic retinopathy. Indian Journal of Ophthalmology 2023;72(Suppl 1):S11-S15. doi:10.4103/ijo.ijo_340_23
49. Wang W, Sun G, Xu A, et al. Proliferative diabetic retinopathy and diabetic macular edema are two factors that increase macrophage-like cell density characterized by en face optical coherence tomography. BMC Ophthalmology 2023;23(1). doi:10.1186/s12886-023-02794-8
50. Al-Nashar HY, Al-Bialy HA. Correlation between foveal microvasculature and inner retinal layer thickness in type 2 diabetes. Delta Journal of Ophthalmology 2022;23(1):50-55. doi:10.4103/djo.djo_13_21
51. Brown NJL, Heathers JAJ. The GRIM Test. Social Psychological and Personality Science 2016;8(4):363-369. doi:10.1177/1948550616673876
52. VanderWeele TJ, Ding P. Sensitivity Analysis in Observational Research: Introducing the E-Value. Annals of Internal Medicine 2017;167(4):268-274. doi:10.7326/m16-2607
53. Sharma S, Karki P, Joshi SN, et al. Influence of glycaemic control on macular thickness in diabetic retinopathy. Endocrinology, Diabetes & Metabolism 2021;5(1). doi:10.1002/edm2.308
54. Doan S, Vo QM, Duong Ha KL. Association between HbA1c level and retinal nerve fiber layer thickness in non-proliferative diabetic retinopathy. Tạp chí Y học Việt Nam 2025;556(2). doi:10.51298/vmj.v556i2.16222
55. Al-Hawasi A, Lagali N. Retinal ganglion cell layer thickness and volume measured by OCT changes with age, sex, and axial length in a healthy population. BMC Ophthalmology 2022;22(1). doi:10.1186/s12886-022-02488-7
56. Rabiolo A, Fantaguzzi F, Montesano G, et al. Comparison of Retinal Nerve Fiber Layer and Ganglion Cell-Inner Plexiform Layer Thickness Values Using Spectral-Domain and Swept-Source OCT. Translational Vision Science & Technology 2022;11(6):27. doi:10.1167/tvst.11.6.27
57. Mohd-Ilham I, Tai ELM, Suhaimi H, et al. Evaluation of Macular and Retinal Nerve Fiber Layer Thickness in Children with Type 1 Diabetes Mellitus without Retinopathy. Korean Journal of Ophthalmology 2021;35(4):287-294. doi:10.3341/kjo.2020.0106
58. Yu Q, Xiao Y, Lin Q, et al. Two-year longitudinal study on changes in thickness of the retinal nerve fiber layer and ganglion cell layer in children with type 1 diabetes mellitus without visual impairment or diabetic retinopathy. Current Eye Research 2022;47(8):1218-1225. doi:10.1080/02713683.2022.2079142
59. Kim JT, Lee MW. Longitudinal changes in each retinal layer thickness in patients with moderate or more severe diabetic retinopathy taking calcium dobesilate. PLOS One 2025;20(6):e0325655. doi:10.1371/journal.pone.0325655
60. Sung JY, Kim JT, Lee MW. Longitudinal changes in each retinal layer thickness in diabetic retinopathy patients treated with pan-retinal photocoagulation. Eye 2025;40(3):376-382. doi:10.1038/s41433-025-04173-7
61. Fan Y, Li Y, Li L, et al. Longitudinal Association of Decreased Serum Uric Acid Level with the Thinning of Ganglion Cell Inner Plexiform Layer Thickness in Chinese Adults with Type 2 Diabetes Mellitus without Retinopathy. Current Eye Research 2025;50(10):1045-1053. doi:10.1080/02713683.2025.2517301
62. Yu HY, Kim JJ, Kim JT, et al. Impact of systemic hypertension on inner retinal layer thickness and macular microvasculature in patients with diabetic retinopathy. Acta Diabetologica 2024;62(2):271-279. doi:10.1007/s00592-024-02355-5
63. Sung JY, Kim JJ, Hwang JY, et al. Retinal neurodegeneration in diabetic retinopathy with systemic hypertension. Acta Diabetologica 2024;61(4):495-504. doi:10.1007/s00592-023-02226-5
64. Fernández-Espinosa G, Orduna-Hospital E, Sopeña-Pinilla M, et al. Tracking Macular Sensitivity and Inner Retinal Thickness in Long-Term Type 1 Diabetes: A Five-Year Prospective Examination in Patients without Diabetic Retinopathy. Life 2024;14(9):1152. doi:10.3390/life14091152
65. Damian I, Nicoară SD. Correlations between Retinal Arterial Morphometric Parameters and Neurodegeneration in Patients with Type 2 Diabetes Mellitus with No or Mild Diabetic Retinopathy. Medicina 2021;57(3):244. doi:10.3390/medicina57030244
66. Li Z, Yang F, Deng X, et al. Associations Between Choroidal Alterations and Early Neurodegeneration in Diabetes Without Diabetic Retinopathy. Retina 2024;44(8):1288-1297. doi:10.1097/iae.0000000000004126
67. Özata Gündoğdu K, Doğan E, Çelik E, et al. Retinal nerve fiber layer and ganglion cell complex thickness in diabetic smokers without diabetic retinopathy. Cutaneous and Ocular Toxicology 2023;43(1):22-26. doi:10.1080/15569527.2023.2268162
68. Dwijayanti S, Irfani I, Sirait SN, et al. Relationship of Peripapillary Retinal Perfusion with Peripapillary Retinal Nerve Fiber Layer Thickness in Diabetes Mellitus Patients without Diabetic Retinopathy. International Journal of Retina 2021;4(2):119. doi:10.35479/ijretina.2021.vol004.iss002.161
69. Halim A, Syumarti S, Rini M, et al. Prevalence and Associated Factors of Diabetic Retinopathy in People with Type 2 Diabetes Attending Community Based Diabetic Retinopathy Screening in Greater Bandung, Indonesia. International Journal of Retina 2022;5(1):1. doi:10.35479/ijretina.2022.vol005.iss001.172
70. ElSayed NA, McCoy RG, Aleppo G, et al. 12. Retinopathy, Neuropathy, and Foot Care: Standards of Care in Diabetes-2025. Diabetes Care 2025;48(Supplement_1):S252-S265. doi:10.2337/dc25-s012
71. Lim JI, Kim SJ, Bailey ST, et al. Diabetic Retinopathy Preferred Practice Pattern®. Ophthalmology 2025;132(4):P75-P162. doi:10.1016/j.ophtha.2024.12.020
72. Shukla B, Nidhi, Priya, et al. Determination of the association of ganglion cell-inner plexiform layer and retinal nerve fiber layer thickness with different grades of myopia: A spectral domain OCT-based study. EyeQuest 2022;47(2):45. doi:10.4103/equest.equest_4_23
73. Abera A, W. Gessesse G. Diagnostic performance of optical coherence tomography macular ganglion cell inner plexiform layer and retinal nerve fiber layer thickness in glaucoma suspect and early glaucoma patients at St. Paul's hospital millennium medical college, Addis Ababa, Ethiopia. PLOS ONE 2023;18(1):e0263959. doi:10.1371/journal.pone.0263959